Revisiting the role of calcite in Spondylus crassisquama shell

Article *in* Bioinspired, Biomimetic and Nanobiomaterials · December 2017

DOI: 10.1680/jbibn.16.00032

5 authors, including:

Sol Angel Rodriguez Carrillo
Pontifical Catholic University of Peru
14 PUBLICATIONS **215** CITATIONS
SEE PROFILE

Fernando G Torres
Pontifical Catholic University of Peru
121 PUBLICATIONS **4,374** CITATIONS
SEE PROFILE

Marta Fernández-García
Spanish National Research Council
243 PUBLICATIONS **6,726** CITATIONS
SEE PROFILE

Daniel López
Instituto de Ciencia y Tecnología de Polímeros
149 PUBLICATIONS **3,736** CITATIONS
SEE PROFILE

Rodriguez S, Brañez LE, Torres FG, Fernández-García M and López D (2016) Revisiting the role of calcite in *Spondylus crassisquama* shell. *Bioinspired, Biomimetic and Nanobiomaterials*, http://dx.doi.org/10.1680/jbibn.16.00032

Bioinspired, Biomimetic and Nanobiomaterials

Research Article
Received 07/09/2016 Accepted 12/12/2016
Keywords: composite materials/mechanical properties/natural materials

ice | science

ICE Publishing: All rights reserved

ice Institution of Civil Engineers publishing

Revisiting the role of calcite in *Spondylus crassisquama* shell

1 **Sol Rodriguez** MEng
PhD candidate, Department of Mechanical Engineering, Pontificia Universidad Católica del Perú, Lima, Peru

2 **Luz E. Brañez** MEng
Research Assistant, Department of Mechanical Engineering, Pontificia Universidad Católica del Perú, Lima, Peru

3 **Fernando G. Torres** PhD*
Professor, Department of Mechanical Engineering, Pontificia Universidad Católica del Perú, Lima, Peru

4 **Marta Fernández-García** PhD
Researcher, Instituto de Ciencia y Tecnología de Polímeros – Consejo Superior de Investigaciones Cientificas, Madrid, Spain

5 **Daniel López** PhD
Director, Instituto de Ciencia y Tecnología de Polímeros – Consejo Superior de Investigaciones Cientificas, Madrid, Spain





***Spondylus crassisquama* (*princeps*) is a bivalve mollusc inhabiting the coast of Central and South Americas. Its shell uses a two-layer armour system to protect the inner soft tissues from the environment. The external layer is composed of a calcite-based composite, and the internal layer is composed of an aragonite-based composite. For the first time, the structural characterisation of the *S. crassisquama* shell is reported. The results show similarities with those for other shells such as that of red abalone. As expected, microhardness tests demonstrate that the internal nacreous layer is stiffer and harder than the external calcitic layer. However, the amount of energy dissipated during the indentation tests of the calcitic layer is similar to the amount of energy dissipated by the nacreous layers. Despite the highly ordered structure of the nacreous layer, the characterisation conducted shows that the calcitic layer can also be used as a model for the development of bioinspired materials.**

1. Introduction

Animals are composed of a plethora of natural materials with remarkable properties. The hierarchical structures of some natural materials, such as bones,[1] body armour[2] and shells,[3] have components that work in a synergistic way. These natural composites, in general, exhibit a more effective and efficient mechanical behaviour when compared to their isolated components. Natural composite materials combine high levels of mechanical resistance with toughness, properties that cannot be easily achieved by artificial means.[4]

Spondylus crassisquama is a mollusc from the bivalve family that is rather large (height up to 170 mm) and heavy (over 2 kg).[5] It is found along the Pacific coast of the Americas, from Baja California to the north, extending south to Peru[6] and is commonly found affixed to coral and rocks at depths up to 30 m.[5]

Shells of gastropods and bivalves are composite materials containing a mineral phase embedded in organic matrices.[7] The mineral phase comprises aragonite (nacreous shells) or calcite (calcitic shells). Some species are bilayered, displaying an internal layer of aragonite and an external layer of calcite.[8] The nacreous layer is formed by sheets of calcium carbonate ($CaCO_3$) in the form of aragonite tablets, while the calcitic layer is formed by calcium carbonate in the form of elongated single-crystal prisms of calcite.[7,9,10]

Nacre, also known as mother of pearl, is made from aragonite, a brittle ceramic.[11] Aragonite makes up 95% of its total volume, with the remaining 5% formed by a thin layer of proteins and polysaccharides.[3,12] The study of the mechanical properties of nacre has shown that it outperforms its individual constituents.[3,13] According to Zhang *et al.*,[14] the fracture toughness of nacre is about 3000 times higher than that of aragonite. This is due to the 'brick-and-mortar' structure of nacre in which aragonite platelets (bricks) are held together by adhesive proteins (mortar). This structure inhibits crack propagation and explains the impressive fracture resistance of nacre. There is abundant information in the literature regarding the mechanical response of nacre to a variety of testing, including tensile,[3,15–17] shear,[3,17,18] flexion[16,19] and compression tests,[19,20] as well as microindentation[19,21] and nanoindentation tests.[22–24]

Due to its hardness, the external calcite layer provides protection against predators.[7,13] Some studies have reported the mechanical properties of the calcite layer by using nanoindentation tests.[25,26]

***Corresponding author e-mail address:** fgtorres@pucp.pe

However, it is nacre rather than calcite that has attracted most of the attention in studies addressing these materials. According to Scopus, there are around 200 papers describing the structure of nacre and no more than 35 that partially describe the calcite layer. In 2015–2016, ten papers reported the development of new materials inspired by the structure of nacre, prepared through the integration of ceramic reinforcements into polymeric matrices.

Novel nacre-inspired materials were developed employing ceramics such as zirconium dioxide (ZrO_2)[27] and silicon carbide (SiC)[28] in platelet form, bonded by glues. These materials exhibit a non-brittle behaviour and an increased toughness in comparison to those of pure ceramics. A few additional studies addressed shells in order to develop new materials for tissue engineering, notably for bone regeneration.[29] Nacre has demonstrated suitable properties for this application, including its compressive strength and protein adsorption capacity.[30] Some studies demonstrate a synergistic effect between hydroxyapatite and aragonite for biocompatibilisation in bone regeneration.[31]

This paper compares the local mechanical properties of the calcite and nacre layers in the shells of *S. Crassisquama*. The structure–property relationships in the calcite layer are focused on, with a special emphasis on the energy dissipation mechanisms. This work aims to show that other structures different from the layered constructs found in nacre can also display interesting energy dissipation mechanisms accompanied by high toughness.

2. Experimental

2.1 Materials

S. crassisquama (*princeps*) shells were obtained from the northern Peruvian coast. They were washed with distilled water to remove sand, salt and impurities and were stored in a desiccator.

2.2 Characterisation techniques

Attenuated total reflection Fourier transform infrared (IR) spectroscopy (FTIR) tests were performed in a PerkinElmer Spectrum One spectrophotometer. The shells were cut and the samples were ground to powder. A mixture of the powdered shell and potassium bromide (KBr) were compressed into pellets. For each test, an average of eight scans at a resolution of 4 cm^{-1} in a range from 4000 to 650 cm^{-1} were recorded. The data were analysed by means of the IR Expert software.

A Renishaw inVia Reflex Raman system coupled to an optical microscope was used to record spectra from the samples. A 785-nm IR diode laser was focused on the sample with a ×100 microscope objective. For each sample, eight scans were recorded in the 3500–500 cm^{-1} spectral range with a resolution of 4 cm^{-1} by using an exposure time of 10 s.

X-ray diffraction (XRD) spectra were recorded using a Bruker D8 diffractometer with a copper (Cu) laser and a Vantec-1 detector. Nickel (Ni)-filtered copper Kα radiation (wavelength of 1·5406 A) was produced at 40 kV and 40 mA. Scattered radiation was detected in the angular range of 10–60° (2θ) with a sampling interval of 0·02°. The data were analysed using specialised software (Analyze and DRXWin).

Thermogravimetric analysis (TGA) was performed by using a PerkinElmer TGA 4000 thermogravimetric analyser. Powdered samples were heated from 30 to 900°C at a heating rate of 10°C/min. The sample weight was plotted as a function of temperature for all samples. Tests were run in triplicate. All measurements were carried out under a nitrogen atmosphere (20 ml/min).

Morphology was examined using a Philips XL 30 scanning electron microscope (SEM). The samples were cleaned with ozone and coated with an 80:20 gold (Au)/palladium (Pd) alloy by using a Polaron SC7640 sputter coater before being placed into the SEM. The tests were carried out in a high vacuum with a voltage of 25 kV and a working distance in the range of 10–20 mm.

An atomic force microscope (AFM) was also used to assess the morphology of samples. A Nanosurf easyScan 2 AFM in the contact mode was used. A cantilever with a nominal spring constant of 0·2 N/m, a resonance frequency of 13 kHz and a tip radius of less than 10 nm were used.

Microhardness tests were performed in a Shimadzu DHU-211 ultra-micro hardness tester. Three samples were cut from the cross-section and mounted in epoxy resin. Then, the mounted samples were progressively polished using standard polishing equipment and deformed by a Berkovich indenter (tip radius 5 μm). The tests were performed at room temperature (~20°C), at a controlled load (100 mN) and at a loading speed of 13·324 mN/s. The tests were repeated at least three times. The elastic modulus and hardness of the samples were recorded.

Cyclic microindentation tests were performed in a BioDent reference point indentation (RPI) instrument (Active Life Scientific).

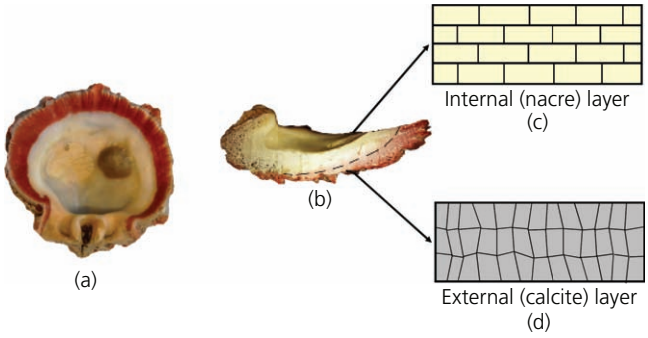

Figure 1. (a) General view of a *S. crassisquama* shell. (b) The cross-sectional view shows a red external layer covering a white nacreous internal layer. (c) The internal layer (nacre) is formed by aragonite platelets in a 'brick-and-mortar' arrangement, (d) while the external layer is formed by prismatic calcite

The RPI technique employs a reference probe that rests on the surface of the sample and a conical indentation probe that repetitively indents the sample in a single location. Three samples from the shell's cross-section were mounted on acrylic resin stubs and polished before testing. Five indentations were assessed in each section. For each test, ten cycles of a 2-N indentation force were applied at a frequency of 2 Hz. Each cycle was formed in three stages. In the first stage, the force is applied until reaching a maximum load of 2 N at a constant load rate (0·5 N/s). In the second stage, the force is held at 2 N, and in the last stage, the force decreases from 2 to 0 N. The average energy dissipated (AED) was recorded. The energy dissipated during an indentation is quantified by measuring the area under the force–displacement curve so that the AED is the average value of the energy dissipated in each cycle.

3. Results

Figure 1(a) shows the internal surface of a representative *Spondylus* shell. Red and white areas are depicted. The cross-sectional view (Figure 1(b)) shows that the red area corresponds to the exterior calcitic layer (Figure 1(d)), and the white area is formed by the interior nacreous layer (Figure 1(c)). The red colour of the calcitic layer is similar to the colour of the external layer of abalone shell.[32] The thickness of the external layer varies along the cross-section from 5 to 15 mm.

Zaremba *et al.*[33] studied the two-layer structure of red abalone shell. They reported a layer of oriented prismatic calcite that grows in a 1–3-mm-wide growth band on the margin of the shell's inner lip. This calcite was reported to comprise prism-shaped aggregates of uniformly oriented 0·1–0·2-μm-dia. acicular

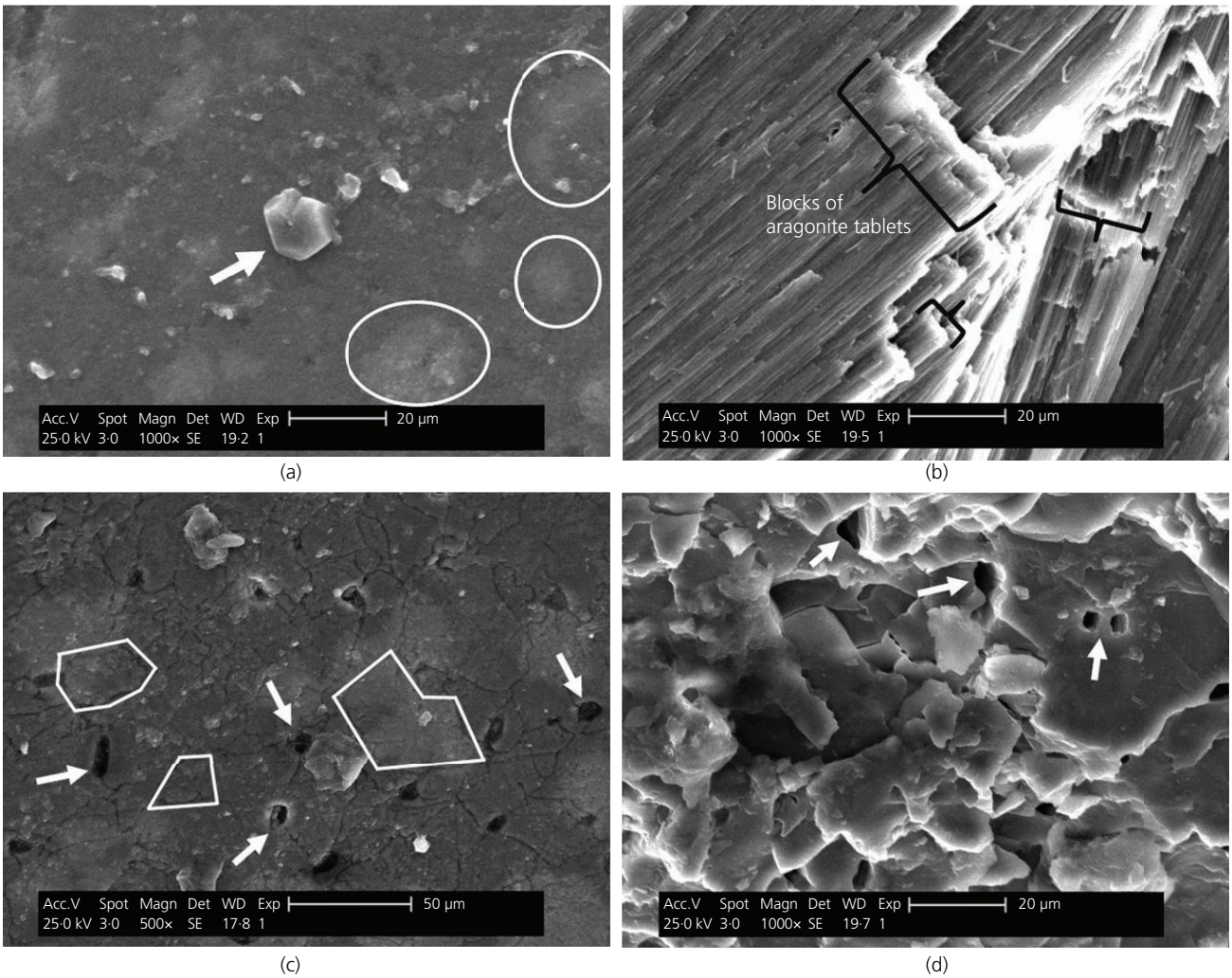

Figure 2. (a) SEM micrograph of the internal nacreous layer (×1000). The white arrow shows a hexagonal inclusion on the surface. White circles/ellipses show inclusions over the surface. (b) Cross-sectional view of the nacreous layer after cryogenic fracture (×1000). Blocks of aragonite tablets are depicted. (c) SEM micrograph of the calcite layer surface (×500). White arrows show pores. Polygonal lines are used to show the limit of calcite platelets. (d) Cross-sectional view of the calcite layer after cryogenic fracture (×1000). White arrows show pores on the fracture surface

crystallites,[34] known as polycrystalline prisms. The red colour of prismatic calcite is due to metabolites.[35]

Each layer was examined by SEM. Figure 2(a) shows the internal nacreous layer. Small pieces of nacre are incrusted over the surface, and some inclusions have a pseudo-hexagonal shape. Figure 2(b) shows a cross-sectional view of the internal layer after cryogenic fracture. The typical brick-and-mortar structure[13,14] composed of 'bricks' of highly oriented aragonite platelets surrounded by an organic matrix is observed. The aragonite platelets are 225–325 nm thick. Nacreous layers from different sources show similar characteristics. The structure of the platelets may vary along the thickness of the shell walls, mainly fluctuating in the content and distribution of the organic matrix and the presence of inclusions.[14]

Figure 2(c) depicts the morphology of the external calcite layer. Grains formed by prismatic calcite platelets are observed along with pores distributed along the surface. According to Sun and Bhushan,[26] these pores may be produced by soft aggregates of protein or sand incrusted during the formation of this external layer. The calcite grains show a non-organised structure that contrasts with that of the aragonite tablets. Figure 2(d) shows the calcite layer surface after cryogenic fracture. Individual calcite grains and interprismatic sinuous grooves are both observed.[36]

AFM images show the two-dimensional and three-dimensional (3D) topography of the external calcite layer. Round grains of calcite (Figure 3) are depicted. According to Li and Zeng,[37] the orientations and observation locations influence the shape of the calcite grains. Three typical types of calcite microstructures were observed: foliated/needle, round and facet-shaped. As similarly shown by the SEM image (Figure 2(d)), the grains are shown to have an irregular morphology and are porous.

In contrast, the surface morphology of the nacreous layer shows a regular structure composed of blocks of aragonite that are surrounded by organic components (Figure 4). Moreover, the 3D

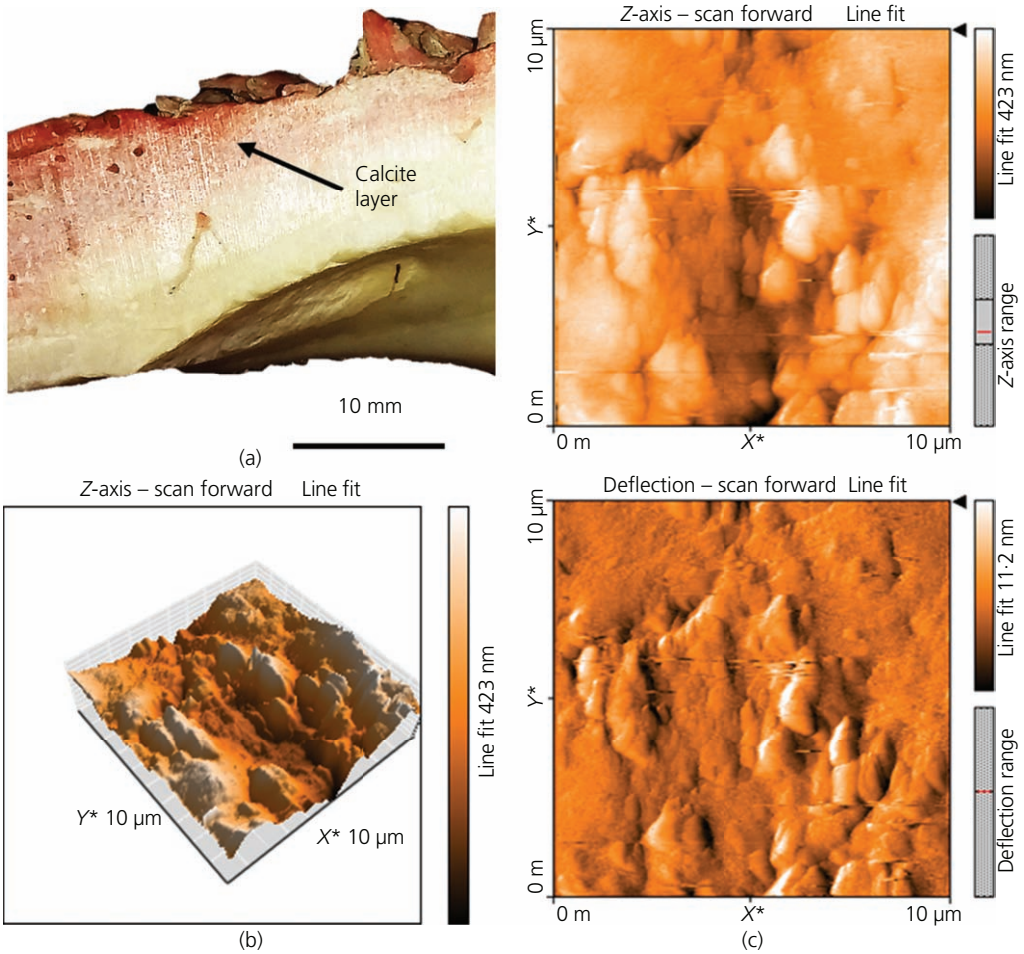

Figure 3. AFM images of the calcite layer of *S.* shell. (a) The cross-sectional macro view of the shell shows the location of the calcite layer. A 3D representation of the external morphology of the calcite layer is shown in (b), together with the surface topography (c)

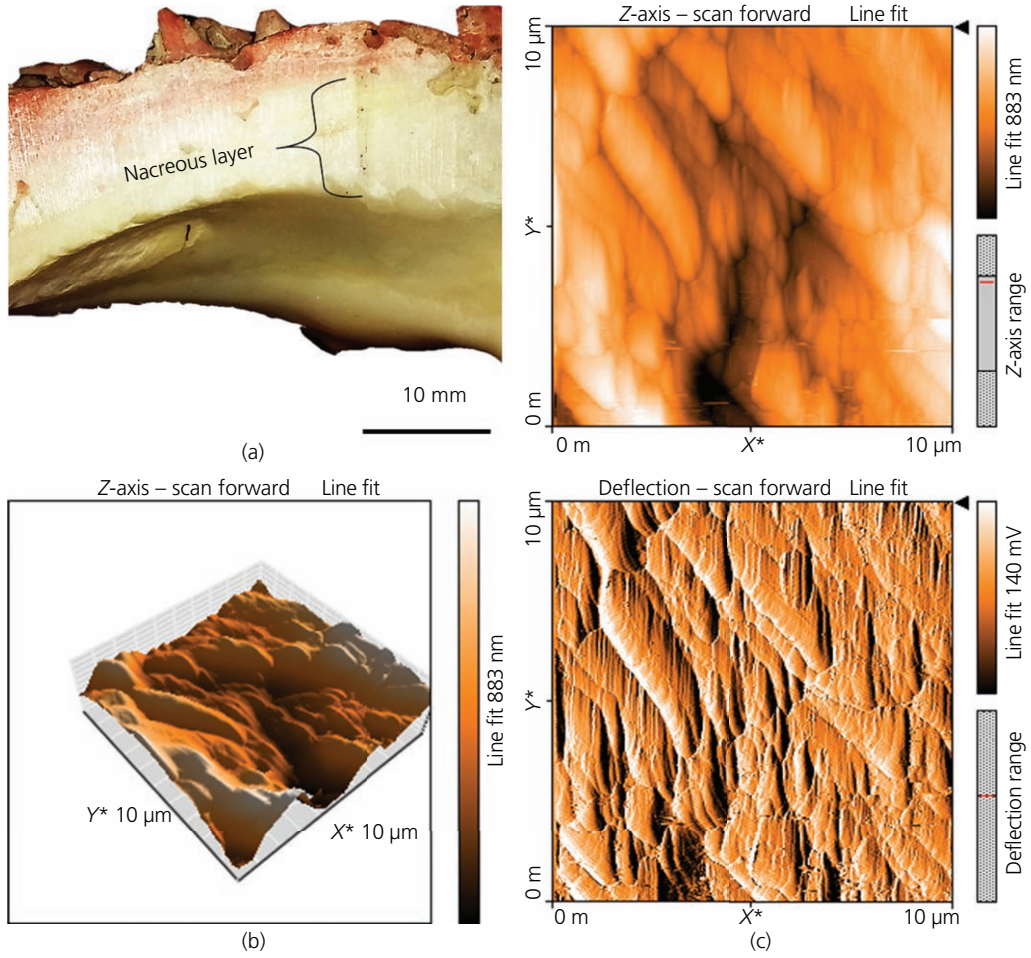

Figure 4. AFM images of the nacreous layer of *S. crassisquama* shell. (a) The external view of the shell shows the position of the nacreous layer. A 3D representation of the external morphology is shown in (b), together with the surface topography (c)

image (Figure 4(b)) suggests that the platelets are thick tablets that are distributed over the entire nacreous layer. Barthelat and Espinosa[3] and Barthelat[38] concluded that aragonite platelets are 3D arrangements of aragonite nanograins. This mode of distribution increases the toughness of the nacre.

Nacre and calcite are two different allotropic forms of calcium carbonate. This is confirmed by the fact that their FTIR spectra are similar (Figure 5). The internal nacreous layer has bands from 4000 to 500 cm^{-1}. The carbonate (CO_3^{2-}) ions in the mineral phase were shown by the internal vibration modes of carbonate ions at 700, 713 (aragonite), 859, 1083 and 1469 cm^{-1}. Balmain *et al.*[9] proposed that the bands in the 2520–2650 cm^{-1} region are contributed by bicarbonate (HCO_3^-) groups due to the absorption of hydroxyl groups (expected around 2600 cm^{-1}). These groups are most likely present in the soluble components of the organic matrix and in the organic–mineral interface. Sabbides and Koutsoukos[39] and Lee *et al.*[40] concluded that signals at 1788 and 1083 cm^{-1} are bands that characterise aragonite. Other bands are attributed to the matrix. The 1473 cm^{-1} signal is characteristic of carboxylate groups, most likely acidic carboxylic amino acids (aspartic and glutamic acids). The O–H and/or N–H stretching modes of the organic matrix components were found in the 3000–3500 cm^{-1} region, while the C–H stretching modes were assigned to the 2800–3000 cm^{-1} region.[9]

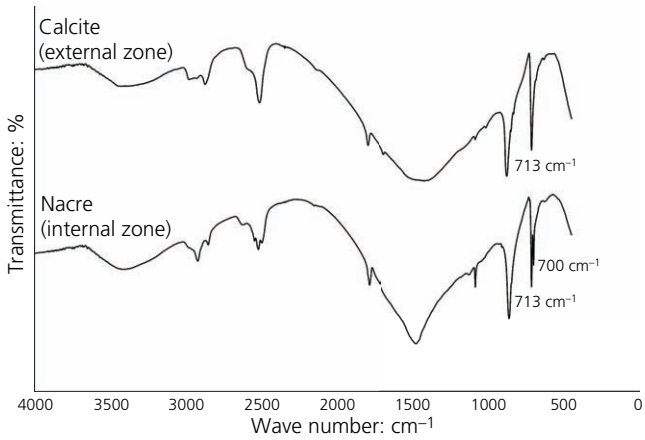

Figure 5. FTIR spectra of the nacreous layer and calcitic layers in *S. crassisquama* shell

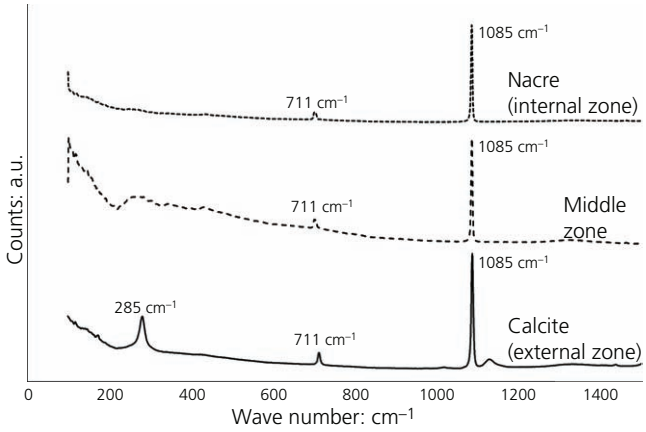

Figure 6. Raman spectra of the nacreous layer and calcite layer taken in the middle and external zones of the shell's cross-section

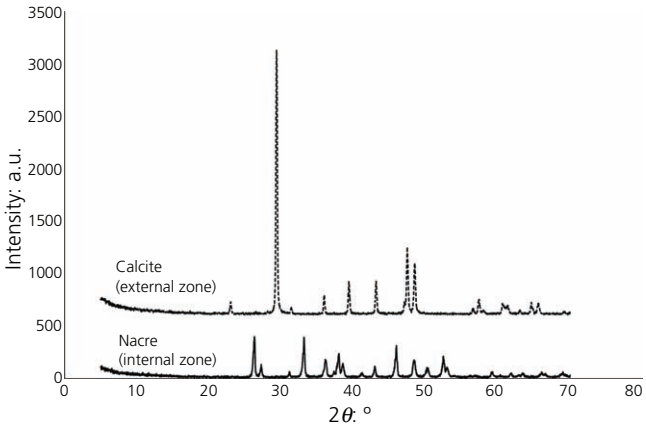

Figure 7. XRD diffractograms of the nacreous and calcite layers in *S. crassisquama* shell

The spectrum of the external calcite layer (solid line, Figure 5) displays the vibrational models of calcium carbonate at 713 and 876 cm^{-1}. A soft signal is detected at 1652 cm^{-1} and is assigned to amide I groups (related to chitin content). The signal at 1083 cm^{-1} is weaker in comparison to that of nacre due to the lower level of aragonite present.[41] Notably, the signal at 700 cm^{-1} disappeared due to the absence of aragonite.

Raman spectra are depicted in Figure 6. The nacreous layer shows signals at 1085 cm^{-1} (symmetric stretching mode of carbonate ions) and 706 cm^{-1} (in-plane bending of carbonate ions), which is in agreement with reported aragonite spectra.[42] The calcite layer has the same signals at 1085 and 711 cm^{-1} and a weak signal at 1445 cm^{-1} that corresponds to the asymmetric stretching of carbonate ions. Additionally, lattice-structured calcite is detected at 285 cm^{-1}.[43]

Calcite and aragonite are two allotropic forms of calcium carbonate. Calcite has a rhombohedral crystal structure, whereas aragonite has an orthorhombic crystal structure. X-ray tests can be used to determine the presence of aragonite and calcite. X-ray diffractograms are shown in Figure 7. The internal layer has the same pattern as aragonite (Joint Committee on Powder Diffraction Standards (JCPDS) file number 50453), which is similar to the results of many studies examining the nacre from other oysters.[44–46] The calcite layer exhibited characteristic peaks (JCPDS file number 05-0586). Based on the (104) diffraction peak (2θ = 29°), the crystal size of calcite was calculated as approximately 37·9 nm by the Scherrer equation. This value is less than results reported by Liu *et al.*[47] for the shell of *Pinctada fucata*. This difference could be accounted by the different amount of protein on *S. crassisquama* calcite. According to Weber *et al.*,[48] the crystal size depends on the amount of protein around the calcite crystals. This diffractogram confirms that the calcite layer exhibits prismatic growing, as suggested by the SEM tests.

TGA tests were performed in order to assess the thermal stability of nacre and calcite (Figure 8). Upon heating, calcium carbonate undergoes a reaction where bound carbon dioxide (CO_2) is released from the material and only calcium oxide (CaO) remains

1. $CaCO_3 \rightarrow CaO + CO_2$

The stoichiometric proportion of calcium oxide and carbon dioxide are 56 and 44%, respectively. The results show that the remaining weight is near the theoretical calculation performed as if the sample were 100% calcite or aragonite (without organic matrix). This confirms that a high percentage of the mass of the samples is composed of the mineral phase.

According to the calculated reduction in the weight of nacre in Figure 8, the content of organic matrix and integrated water is about 1·2% of the total weight. The decomposition of nacre occurs in four steps. The first step (from 30 to 300°C) is related to the moisture evaporation and the initial depolymerisation of organic matrix. The second step (between 300 and 350°C) is related to the diffusion and

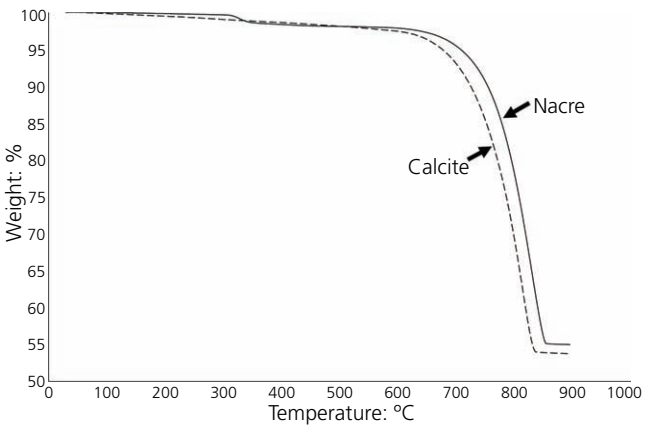

Figure 8. TGA thermograms of nacre (solid line) and calcite (dashed line)

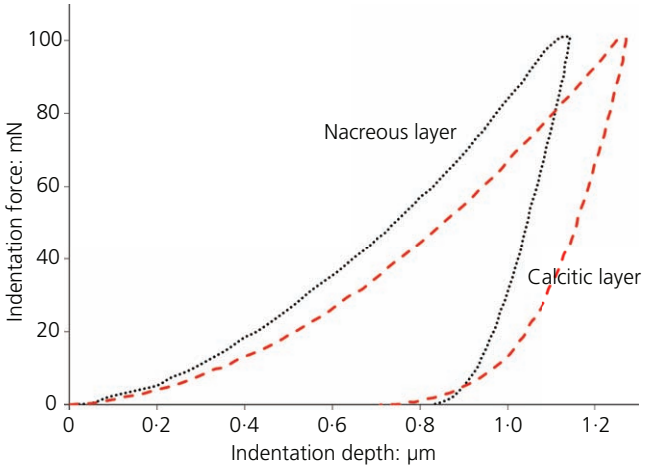

Figure 9. Representative force–penetration depth curves of the calcitic and nacreous layers

evaporation of water incorporated into the orthorhombic structure of aragonite.[49] This water loss is about 0·6–0·7%. The third step occurs from 350 to 600°C, and the weight remains constant. Normally, at these temperatures, organic compounds decompose (carbonise). Finally, the 43–44% reduction in the weight the nacre at 600–800°C is caused by the decomposition of calcium carbonate into calcium oxide and carbon dioxide. When the temperature is raised further, the residual weight remains constant. It is thus concluded that the content of inorganic aragonite is about 98·2% (w/w). After the thermal decomposition, residues of aragonite were 55·3 ± 0·42%.

The calcite layer showed a slightly different thermal decomposition behaviour (Figure 8). First, the matrix decomposition (between 100 and 600°C) occurs in one step with a weight loss of about 1·5%. As described earlier, the structure of calcite contrasts starkly with that of aragonite. Its prismatic structure does not allow for the inclusion of water. Therefore, the weight loss observed is attributed to the degradation of hardened proteins acting as pigments or matrix constituents. Similarly as the nacre layer, the calcite layer has a significant weight loss of 43–44% due to the decomposition of carbonate (explained earlier), and the residues were 53·8 ± 0·93%.

A microindenter was used to measure the hardness, dissipated energy and elastic modulus of the calcitic and the nacreous layers. Figure 9 shows representative force–penetration depth curves of the tests performed on the nacreous and the calcitic layers. It can be observed that the indentation depth is higher for the calcitic layer than that for the nacreous layer. The initial slope of the unloading curves, which is related to the elastic modulus of the sample, is higher for the nacreous layer. Table 1 shows the hardness, the dissipated energy (area below the force–penetration depth curve) and the measured elastic modulus. The external nacreous layer had the highest elastic modulus and hardness values, whereas the calcitic layer exhibited the lowest hardness and elastic modulus. These results are in agreement with the results reported for shells from *Mytilus edulis*, *Haliotis rufescens*, *Pinctada maxima* and *Novocrania anomala*. In these studies, the nacreous layer has the highest hardness and elastic modulus.[50–52]

Notably, the AED by the calcite layer was 0·0427 μJ compared to 0·0380 μJ for the aragonite layer. Microindentation tests carried out using a cyclic indentation technique (RPI) with an indentation force of 2 N exhibit concordant results. The energy dissipated by the calcite layer in the RPI tests was in the range of 1·5–1·7 μJ, whereas the energy dissipated by the aragonite layer was in the range of 1·3–1·9 μJ.

Values of hardness and elastic modulus for nacre were compared to values obtained from the literature for nanoindentation. While standards for the *Spondylus* shell have not been previously established, drawing comparisons with Table 2, the authors' studies demonstrate a response similar to that of red abalone.

Table 1. Hardness, dissipated energy and elastic modulus of *Spondylus* shell microindentation tests

	Hardness: GPa	Dissipated energy: μJ	Elastic modulus: GPa
External calcite layer	2·87 ± 0·15	0·043 ± 0·003	56·24 ± 1·16
Internal nacreous layer (middle)	3·64 ± 0·80	0·038 ± 0·002	64·20 ± 16·51
Internal nacreous layer (end)	4·14 ± 0·40	0·038 ± 0·006	74·43 ± 8·77

Table 2. Values of hardness and elastic modulus for nacre from other species measured by nanoindentation

Sample	Hardness: GPa	Elastic modulus: GPa	References
Pinctada maxima	—	54·4–62·5	Stempflé *et al.*[24]
Lamprotula fibrosa	3·42	59·6	Sun and Tong[23]
Green mussel (*Perna canaliculus*)	4·5	59·6	Leung and Sinha[53]
	—	147	Moshe-Drezner *et al.*[54]
Red abalone (*Haliotis rufescens*)	7·5	79	Barthelat *et al.*[22]
	2–4	60–80	Ries[55]
	0·69–19·32	14·9–113·7	Katti *et al.*[56]
	1·32–3·21	40·95–56·71	Lin and Meyers[57]
	—	70–114	Bezares *et al.*[58]
Trochus niloticus	8·7–10·8	103–114	Bruet[59]

However, mechanical properties of nacre depend on a plethora of factors including but not limited to tablet length and thickness, grain size and the nature of its organic matrix.

4. Discussion

Nacre is a heterogeneous medium that retards crack propagation and has been reported to be 3000 times as tough as its constituents (aragonite and adhesive polymers).[56] According to Wang *et al.*,[13] cracks tend to propagate towards the region with lower elastic modulus. In nacre, this region is composed of an organic matrix and regions with inclusions. Failure paths have winding trajectories, determined by the arrangement (tablets in bricks) and distribution (brick structure) of platelets. This demonstrates the protective function of the organic matrix against deformation (dissipation of deformation energy) and recovery (platelets do not fail, and the matrix can be regenerated).[60]

In the past, the calcite layer has not received much attention as a structural component of bivalve shells. One claim is that the main function of the calcite layer, rather than to provide mechanical support, is to provide protection against the dissolution of the nacre. As described by Harper[61] and Ries,[55] the calcite layer is an effective adaptation to prevent the dissolution of aragonite in unsaturated waters, also called 'calcite seas' (molar magnesium (Mg)/calcium (Ca) < 2). Moreover, the external layer is 50–70% harder than geologic calcite and is useful for protection against natural predators and mechanical impacts.[7]

Despite the impressive resistance to fracture reported for nacre in the literature, the tests carried out in this study show that nacre and calcite have similar mechanical properties. The hardness and elastic modulus of nacre are higher than those of calcite. In contrast, the dissipated energy of calcite is similar to the dissipated energy of nacre.

It should be noted that the microindentation technique used here is not usually employed to determine the toughness of materials. However, previous studies have used indentation tests to quantify the toughness of materials. Anstis *et al.*[62] and Chantikul *et al.*[63] developed a procedure to use the crack traces on the indented surfaces of ceramics tests to evaluate their fracture toughness. Their results suggest that the energy dissipated during indentation tests can provide an indication of the toughness of solid materials. Further exploration of the external (calcitic) layer of the *Spondylus* shell could provide novel criteria for the development of bioinspired materials.

5. Conclusions

Chemical and physical characterisation of the *S. crassisquama* shell confirmed that it mainly consists of calcium carbonate (98% w/w) with an organic protein matrix. Calcium carbonate is presented in two allotropic forms: calcite and aragonite. The tests performed showed that the hardness and elastic modulus of nacre is higher than those of calcite. Moreover, while the nacreous layer has a modulus higher than that of the calcitic layer, the energy dissipation behaviours of these two layers are similar. This suggests that the structure of calcite can also be a promising source of inspiration for the development of novel biomimetic materials.

Acknowledgements

The authors would like to thank the vice-rectorate for research of the Pontificia Universidad Católica del Perú and the Peruvian Council of Science and Technology (Consejo Nacional de Ciencia, Tecnología e Innovación Tecnológica–Fondo Nacional de Desarrollo Científico y Tecnológico) for financial support. Dr Vicente Lorenzo from the Polytechnical University of Madrid is acknowledged for providing technical support during the microhardness tests.

REFERENCES

1. Reznikov N, Shahar R and Weiner S (2014) Bone hierarchical structure in three dimensions. *Acta Biomaterialia* **10(9)**: 3815–3826.
2. Chen IH, Kiang JH, Correa V *et al.* (2011) Armadillo armor: mechanical testing and micro-structural evaluation. *Journal of the Mechanical Behavior of Biomedical Materials* **4(5)**: 713–722.
3. Barthelat F and Espinosa HD (2007) An experimental investigation of deformation and fracture of nacre-mother of pearl. *Experimental Mechanics* **47(3)**: 311–324.
4. Bouville F, Maire E, Meille S *et al.* (2014) Strong, tough and stiff bioinspired ceramics from brittle constituents. *Nature Materials* **13(5)**: 508–514.
5. Mackensen AK, Brey T, Bock C and Luna S (2012) *Spondylus crassisquama* Lamarck, 1819 as a microecosystem and the effects of associated macrofauna on its shell integrity: isles of biodiversity or sleeping with the enemy? *Marine Biodiversity* **42(4)**: 443–451.
6. Lamprell K (2006) *Spiny Oysters: a Revision of the Living Spondylus Species of the World*. Jean Lamprell, Brisbane, Australia.
7. Kunitake ME, Mangano LM, Peloquin JM, Baker SP and Estroff LA (2013) Evaluation of strengthening mechanism in calcite single crystals from mollusk shells. *Acta Biomaterialia* **9(2)**: 5353–5359.
8. Dauphin Y, Cuif JP and Salome M (2014) Structure and composition of the aragonitic shell of a living fossil: Neotrigonia (Mollusca, Bivalvia). *European Journal of Mineralogy* **26(4)**: 485–494.
9. Balmain J, Hannoyer B and Lopez E (1999) Fourier transform infrared spectroscopy (FTIR) and X-ray diffraction analyses of mineral and organic matrix during heating of mother of pearl (nacre) from the shell of the mollusk *Pinctada maxima*. *Journal of Biomedical Materials Research* **48(5)**: 749–754.
10. Miyamoto H, Miyashita T, Okushima M *et al.* (1996) A carbonic anhydrase from the nacreous layer in oyster pearls. *Proceedings of the National Academy of Sciences of the United States of America* **93(18)**: 9657–9660.
11. Shao Y, Zhao HP, Feng XQ and Gao H (2012) Discontinuous crack-bridging model for fracture toughness analysis of nacre. *Journal of the Mechanics and Physics of Solids* **60(8)**: 1400–1419.
12. Kakisawa H and Sumitomo T (2011) The toughening mechanism of nacre and structural materials inspired by nacre. *Science and Technology of Advanced Materials* **12(6)**: 1–14.
13. Wang S, Zhu X, Li Q, Wang R and Wang X (2016) Damage-tolerance strategies for nacre tablets. *Journal of Structural Biology* **194(2)**: 199–204.
14. Zhang N, Yang S, Xiong L, Hong Y and Chen Y (2016) Nanoscale toughening mechanism of nacre tablet. *Journal of the Mechanical Behavior of Biomedical Materials* **53**: 200–209.
15. Currey JD (1977) Mechanical properties of the mother of pearl in tension. *Proceedings of the Royal Society of London B: Biological Sciences* **196(1125)**: 443–463.

16. Jackson AP, Vicent JFV and Turner RM (1988) The mechanical design of nacre. *Proceedings of the Royal Society of London B: Biological Sciences* **234(1277)**: 415–440.
17. Wang RZ, Sou Z, Evans AG, Yao N and Aksay IA (2001) Deformation mechanisms in nacre. *Journal of Materials Research* **16(9)**: 2485–2493.
18. Menig R, Meyers MH, Meyers MA and Vecchio KS (2000) Quasi-static and dynamic mechanical response of *Haliotis rufescens* (abalone) shells. *Acta Materialia* **48(9)**: 2383–2398.
19. Hamza S, Slimane N, Azari Z and Pluvinage G (2013) Structural and mechanical properties of the coral and nacre and the potentially of their use as bone substitutes. *Applied Surface Science* **264**: 485–491.
20. Liang Y, Zhao J, Wang L and Li F (2008) The relationship between mechanical properties and crossed-lamellar structure of mollusk shells. *Materials Science and Engineering A* **483–484(15)**: 309–312.
21. Wang RZ, Wen HB, Cui FZ, Zhang HB and Li HD (1995) Observations of damage morphologies in nacre during deformation and fracture. *Journal of Materials Science Letters* **30(9)**: 2299–2304.
22. Barthelat F, Li CM, Comi C and Espinosa HD (2006) Mechanical properties of nacre constituents and their impact on mechanical performance. *Journal of Materials Research* **21(8)**: 1977–1986.
23. Sun J and Tong J (2007) Fracture toughness properties of three different biomaterials measured by nanoindentation. *Journal of Bionic Engineering* **4(1)**: 11–17.
24. Stempflé P, Pantale O, Rousseau M, Lopez E and Bourrat X (2010) Mechanical properties of the elemental nanocomponents of nacre structure. *Materials Science and Engineering: C* **30(5)**: 715–721.
25. Lee SW, Kim YM, Kim RH and Choi CS (2008) Nanostructured biogenic calcite: a thermal and chemical approach to folia in oyster shell. *Micron* **39(4)**: 380–386.
26. Sun J and Bhushan B (2012) Hierarchical structure and mechanical properties of nacre: a review. *RSC Advances* **2(20)**: 7617–7632.
27. Zlotnikov I, Gotman I, Burghard Z, Bill J and Gutmanas EY (2010) Synthesis and mechanical behavior of bioinspired ZrO_2–organic nacre-like laminar nanocomposites. *Colloids and Surfaces A: Physicochemical and Engineering Aspects* **361(1–3)**: 138–142.
28. Yang WS, Biamino S, Padovano E *et al.* (2013) Microstructure and mechanical properties of milled fibre/SiC multilayer composites prepared by tape casting and pressureless sintering. *Materials Science and Engineering: A* **588**: 103–110.
29. Shen Y, Yang S, Liu J *et al.* (2014) Engineering scaffolds integrated with calcium sulfate and oyster shell for enhanced bone tissue regeneration. *ACS Applied Materials and Interfaces* **6(15)**: 12177–12188.
30. Chen J, Huang Y, Su M, Cheng K and Zhao Y (2016) Biomimetic synthesis of oriented aragonite crystals and nacre-like composite materials by controlling the fluid type. *Powder Technology*, http://dx.doi.org/10.1016/j.powtec.2016.05.060.
31. Correa de Almeida A, Rodrigues Pereira da Silva A, Nakamura Filho A, Davi de Carvalho M and Valadao Cardoso A (2015) Nacre compared to aragonite as a bone substitute: evaluation of bioactivity and biocompatibility. *Materials Research* **18(2)**: 395–463.
32. López MI and Meyers MA (2016) The organic interlamellar layer in abalone nacre: formation and mechanical response. *Materials Science and Engineering: C* **58**: 7–13.
33. Zaremba CM, Belcher AM, Fritz M *et al.* (1996) Critical transitions in the biofabrication of abalone shells and flat pearls. *Chemistry of Materials* **8(3)**: 679–690.
34. Mutvei H (1991) Structure of molluscan prismatic shell layers. In *Origin, Evolution, and Modern Aspects of Biomineralization in Plants and Animals* (Crick RE (ed.)). Springer, New York, NY, USA, pp. 137–151.
35. Comfort A (1951) The pigmentation of molluscan shells. *Biological Reviews* **26(3)**: 285–301.
36. Okumura T, Suzuki M, Nagasawa H and Kogure T (2010) Characteristics of biogenic calcite in the prismatic layer of a pearl oyster. *Pinctada fucata. Micron* **41(7)**: 821–826.
37. Li T and Zeng K (2014) Nanoscale elasticity mappings of micro-constituents of abalone shell by band excitation-contact resonance force microscopy. *Nanoscale* **6(4)**: 2177–2185.
38. Barthelat F (2014) Designing nacre-like materials for simultaneous stiffness, strength and toughness: optimum materials, composition, microstructure and size. *Journal of the Mechanics and Physics of Solids* **73**: 22–37.
39. Sabbides TG and Koutsoukos PG (1993) The crystallization of calcium carbonate in artificial seawater; role of the substrate. *Journal of Crystal Growth* **133(1–2)**: 13–22.
40. Lee SW, Jang YN and Kim JC (2011) Characteristics of the aragonitic layer in adult oyster shells, *Crassostrea gigas*: structural study of myostracum including the adductor muscle scar. *Evidence-Based Complementary and Alternative Medicine*, http://dx.doi.org/10.1155/2011/742963.
41. Dauphin Y and Marin F (1995) The compositional analysis of recent cephalopod shell carbohydrates by Fourier transform infrared spectrometry and high performance anion exchange-pulsed amperometric detection. *Experientia* **51(3)**: 278–283.
42. Wehrmeister U, Soldati AL, Jacob DE, Hager T and Hofmeister W (2009) Raman spectroscopy of synthetic, geological and biological vaterite: a Raman spectroscopic study. *Journal of Raman Spectroscopy* **41(2)**: 193–201.
43. Urmos J, Sharma SK and Mackenzie FT (1991) Characterization of some biogenic carbonates with Raman spectroscopy. *American Mineralogist* **76(3–4)**: 641–646.
44. Pokroy B, Desmensky V and Zolotoyabko E (2009) Nacre in mollusk shells as a multilayered structure with strain gradient. *Advanced Functional Materials* **19(7)**: 1054–1059.
45. Zhang G and Xu J (2013) From colloidal nanoparticles to a single crystal: new insights into the formation of nacre's aragonite tablets. *Journal of Structural Biology* **182(1)**: 36–43.
46. Xu J and Zhang G (2015) Unique morphology and gradient arrangement of nacre's platelets in green mussel shells. *Materials Science and Engineering: C* **52**: 186–193.
47. Liu C, Xie L and Zhang R (2015) Heterogeneous distribution of dye-labelled biomineralization proteins in calcite crystals. *Scientific Reports* **5**: 1–8.
48. Weber E, Bloch L, Guth C *et al.* (2014) Incorporation of a recombinant biomineralization fusion protein into the crystalline lattice of calcite. *Chemistry of Materials* **26(17)**: 4925–4932.
49. Földvári M (2011) *Handbook of Thermogravimetric System of Minerals and Its Use in Geological Practice*. Geological Institute of Hungary, Budapest, Hungary.
50. Fitzer SC, Wenzhong Z, Elizabeth Tanner *et al.* (2013) Ocean acidification alters the material properties of *Mytilus edulis* shells. *Journal of the Royal Society Interface* **12(103)**: 1–8.
51. Pérez-Huerta A, Cusack M, Zhu W, England J and Hughes J (2007) Material properties of brachiopod shell ultrastructure by nanoindentation. *Journal of the Royal Society* **4(4)**: 33–39.
52. Li T and Zeng K (2014) Nanoscale elasticity mappings of micro-constituents of abalone shell by band excitation-contact resonance force microscopy. *Nanoscale* **6(4)**: 2177–2185.
53. Leung HM and Sinha SK (2009) Scratch and indentation tests on seashells. *Tribology International* **42(1)**: 40–49.
54. Moshe-Drezner H, Shilo D, Dorogoy A and Zoloyabko E (2010) Nanometer-scale mapping of elastic modules in biogenic composites: the nacre of mollusk shells. *Advanced Functional Materials* **20(16)**: 2723–2728.
55. Ries JB (2010) Review: Geological and experimental evidence for secular variation in seawater Mg/Ca (calcite-aragonite seas) and its effects on marine biological calcification. *Biogeosciences* **7(9)**: 2795–2849.
56. Katti KS, Mohanty B and Katti DR (2006) Nanomechanical properties of nacre. *Journal of Materials Research* **21(5)**: 1237–1242.

57. Lin AYM and Meyers MA (2009) Interfacial shear strength in abalone nacre. *Journal of Mechanical Behavior of Biomedical Materials* **2(6)**: 607–612.
58. Bezares J, Peng ZL, Asaro RJ and Zhu Q (2011) Macromolecular structure and viscoelastic response of the organic framework of nacre in *Haliotis rufescens*: a perspective and overview. *Journal of Theoretical and Applied Mechanics* **38(2)**: 75–106.
59. Bruet BJF (2005) Nanoscale morphology and indentation of individual nacre tablets from the gastropod mollusk *Trochus niloticus*. *Journal of Materials Research* **20(9)**: 2400–2419.
60. Suzuki M, Nakayama S, Nagasawa H and Kogure T (2013) Initial formation of calcite crystals in the thin prismatic layer with the periostracum of *Pinctada fucata*. *Micron* **45**: 136–139.
61. Harper EM (2000) Are calcitic layers an effective adaptation against shell dissolution in the Bivalvia? *Journal of Zoological Society of London* **251(2)**: 179–186.
62. Anstis GR, Chantikul P, Lawn BR and Marshall DB (1981) A critical evaluation of indentation techniques for measuring fracture toughness: I, direct crack measurements. *Journal of the American Ceramic Society* **64(9)**: 533–538.
63. Chantikul P, Anstis GR, Lawn BR and Marshall DB (1981) A critical evaluation of indentation techniques for measuring fracture toughness: II, strength method. *Journal of the American Ceramic Society* **64(9)**: 539–543.